Solution Structure of BmP02, a New Potassium Channel Blocker from the Venom of the Chinese Scorpion *Buthus martensi* Karsch[†,‡]

Yingqi Xu,[§] Jihui Wu,[*,§] Jiming Pei,[§] Yunyu Shi,[*,§] Yonghua Ji,[||] and Qingchun Tong[||]

Laboratory of Structural Biology, School of Life Science, University of Science and Technology of China, Hefei, Anhui 230026, PRC, and Shanghai Institute of Physiology, Chinese Academy of Sciences, Shanghai 200031, PRC

Received April 17, 2000; Revised Manuscript Received August 21, 2000

ABSTRACT: BmP02 is a 28-amino acid residue peptide purified from the venom of the Chinese scorpion *Buthus martensi* Karsch, which had been demonstrated to be a weak blocker of apamin-sensitive calcium-activated potassium channels. Two-dimensional NMR spectroscopy techniques were used to determine the solution structure of BmP02. The results show that BmP02 formed a α/β scorpion fold, the typical three-dimensional structure adopted by most short chain scorpion toxins whose structures have been determined. However, in BmP02 this α/β fold was largely distorted. The α-helix was shortened to only one turn, and the loop connecting the helix to the first β-strand exhibited conformational heterogeneity. The instability of BmP02 could be attributed to a proline at position 17, which is usually a glycine. Because the residue at this position makes intense contact with the α-helix, it was supposed that the bulky side chain of proline had pushed the helix away from the β-sheet. This had a significant influence on the structure and function of BmP02. The α-helix rotated by about 40° to avoid Pro17 while forming two disulfides with the second β-strand. The rotation further caused both ends of the helix to be unwound due to covalent restrictions. According to its structure, BmP02 was supposed to interact with its target via the side chains of Lys11 and Lys13.

Numerous polypeptidic toxins that interfere with the activity of ionic channels and modulate their functional properties have been found in the venom of various scorpions. The accumulated data show that most of the long chain scorpion neurotoxic polypeptides (60−70 amino acid residues, containing four disulfide bridges) are blockers of voltage-gated Na^+ channels (*1*−*3*), while the short chain scorpion neurotoxins (28−39 amino acid residues, containing three disulfide bridges) mainly interact with K^+ or Cl^- channels (*4*−*8*).

Venom of various scorpions had been investigated intensively in hopes of discovering highly selective toxins for the diverse K^+ channels. Many short chain scorpion neurotoxins exhibiting different specificities and potencies for different types of potassium channels were thus discovered (*4*−*8*). Among them, charybdotoxin, kaliotoxin, and noxiustoxin interfere with high-conductance calcium-activated K^+ channels (BK_{Ca} channels)[1] and voltage-gated potassium K^+ channels, while leiurotoxin I acts on low-conductance calcium-dependent K^+ channels (SK_{Ca} channels). Two other scorpion toxins that interact with SK_{Ca} channels are P05 (*9*) and P01 (*10*) from the venom of the scorpion *Androctonus mauretanicus mauretanicus*. P05 is a highly potent blocker of the apamin-sensitive SK_{Ca} channels, and its sequence is 87% identical to that of leiurotoxin I; P01 is a very weak blocker with respect to the same channels.

Many short chain scorpion toxins, including P05 and P01, had been investigated with NMR techniques soon after their characterization (*11*−*16*). These studies revealed a common global folding for all these neurotoxins rectified by three disulfide bridges. Despite their sequence variations, these short chain scorpion toxins all possess a α-helix connected to a two- or three-stranded antiparallel β-sheet by two of the three disulfides. Due to their conformational stability and tolerance to sequence mutations, these short chain scorpion toxins had been used as small scaffolds onto which functional groups from larger proteins could be integrated (*17*−*19*).

BmP02 is a 28-amino acid toxin characterized from the venom of the Chinese scorpion *Buthus martensi* Karsch (*20*, *21*), a species widely distributed in northwestern China, Mongolia, and Korea. Its sequence is 46% similar with that of P01. Like P01, BmP02 exhibited a low toxic activity in mice after intracerebroventricular injection, and competed only weakly ($K_{0.5} > 1\ \mu M$) with iodinated apamin for binding to SK_{Ca} channels (*20*). Recently, it was found that BmP02 was able to reversibly diminish the current of the transient outward K^+ channel (I_{to}) in adult rat ventricular myocytes in a concentration-dependent manner (*21*).

The sequence alignment of BmP02 together with P01, P05, and leiurotoxin I is shown in Figure 1. On the basis of the

[†] This work is supported by the Chinese National Fundamental Research Project, Grant G1999075605, the Chinese National Natural Science Foundation, Grant 39990600, the Foundation of Chinese Academy of Science, and the National Basic Research Program of China, Grant G1999054001.

[‡] The atomic coordinate file of BmP02 has been deposited in the Brookhaven Protein Data Bank (entry 1DU9).

* Corresponding authors. J.W.: fax, +86-551-3603754; e-mail, wujihui@ustc.edu.cn. Y.S.: fax, +86-551-3603754; e-mail, yyshi@ustc.edu.cn.

[§] University of Science and Technology of China.

[||] Chinese Academy of Sciences.

[1] Abbreviations: NMR, nuclear magnetic resonance; SK_{Ca} channel, low-conductance calcium-activated potassium channel; BK_{Ca} channel, high-conductance calcium-activated potassium channel.

10.1021/bi000860s CCC: $19.00
Published on Web 10/21/2000

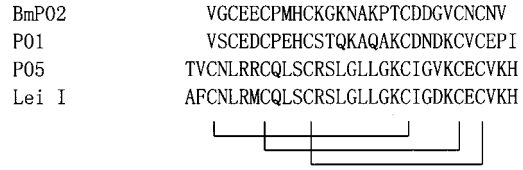

FIGURE 1: Sequence alignment of BmP02 with P01, P05, and leiurotoxin I. The conserved disulfide bridges are shown.

structures, Cys3 of P01 was aligned with Leu5 instead of Cys3 of P05. The two arginines (RR) located at the beginning of the helix in P05, which are believed to be involved in binding to K^+ channels (*15*, *22*), are replaced with two acidic amino acids in both P01 (ED) and BmP02 (EE). This mutation was believed to be the major reason for the decreased affinity of P01 and BmP02 for SK_{Ca} channels. We present the solution structure of BmP02 here, which revealed some unusual features of this molecule.

MATERIALS AND METHODS

Sample Preparation. BmP02 was purified from the venom of *B. martensi* Karsch and characterized as described previously (*21*). The purified peptide was dissolved to a final concentration of 3 mM in 500 μL of H_2O/D_2O (90/10 mixture, v/v). The pH was then adjusted to 4.0 (uncorrected for the isotope effect). After a set of NMR experiments, this sample was lyophilized and dissolved in 99.96% D_2O.

NMR Spectroscopy. All NMR measurements were performed on a Bruker DMX500 spectrometer, and self-shielded *z*-axis gradients were used. The experiments were performed at three temperatures (287, 300, and 310 K) to solve assignment ambiguities. Two-dimensional TOCSY, DQF-COSY, and NOESY spectra were acquired in H_2O and D_2O using the States−TPPI method (*23*) to achieve F_1 quadrature detection. Typically, 700 free induction decays of 2048 data points were collected per experiment. The spectral width was set to 5000 Hz. TOCSY spectra were recorded with a spin-lock time of 80 ms, while mixing times of 80, 100, 150, 250, and 300 ms were used for NOESY to identify spin-diffusion effects. To minimize the contribution from zero-quantum coherence, the NOESY mixing time was varied randomly by 10% (*24*). Low-power presaturation and WATERGATE (*25*) were used to suppress the water signal in these experiments. The amide proton exchange experiments were carried out immediately after dissolution of this peptide into D_2O on an ice bath. The disappearance of NH signals was followed at 283 K. Twenty one-dimensional spectra were acquired continuously over the first half-hour. Then several NOESY spectra, taken at about 0.5, 1, 5, 5, and 5 h, were acquired sequentially.

Data Processing. Spectra were processed with PROSA (*26*) and Bruker's UXNMR software. The matrixes were transformed to a final size of 2048 points in both dimensions. The signal was multiplied by a shifted sine bell window in both dimensions before Fourier transformation. Baseline distortions were corrected using the FLATT procedure.

Spectral Analysis. Spin system identification and sequential assignment were done using the Wüthrich strategy (*27*), aided with the XEASY software (*28*).

Experimental Restraints. NOE intensities were obtained mainly from a NOESY spectrum with a mixing time of 100 ms on the fully protonated sample. For those peaks between two aliphatic protons, with which zero-quantum effects and/or the overlap problem in this spectrum interfered severely, integration was carried out on a NOESY spectrum recorded in D_2O with a mixing time of 300 ms. Buildup curves of the NOE intensity was checked, and no severe spin-diffusion effect was found up to 300 ms (data not shown). The scaling factors for different spectra were chosen carefully after comparing the integration for a set of well-separated strong peaks. All the NOEs were calibrated to distance upper limits according to the well-known r^{-6} relation and known distances, i.e., $d_{\alpha N}$(in a β-strand) = 2.2 Å, d_{NN} = 3.3 Å between two strands of antiparallel β-sheet. To allow for possible fluctuations, the distance restraints derived from side chain cross-peaks and weak backbone cross-peaks were lengthened to 4.0 or 5.0 Å. An additional 0.5 Å was added to those distances corresponding to methyl protons. No lower limit was imposed explicitly.

The $^3J_{HN\alpha}$ values were obtained by measuring the division of cross-peaks on DQF-COSY parallel to F_2 or by using the INFIT routine (*29*) provided by XEASY on NOESY. Then they were converted to ϕ angle constraints as $-65° \pm 35°$ (<6.5 Hz), $-120° \pm 35°$ (>9 Hz), and $-120° \pm 45°$ (>8 Hz).

Structure Calculations. Simulated annealing of the BmP02 structures based on geometric restraints (bond length, bond angle, and improper dihedral angles), simple repulsion nonbonded interactions, and all the restraints (NOE, dihedral angle, and hydrogen bonds) derived from NMR spectra was used in the software "Crystallography & NMR System" (CNS) (*30*). The simulation started from an extended conformation of BmP02 with its disulfide bridges removed. The simulation was carried out in torsion angle space at first, which involved 1000 steps (the time step being 0.015 ps) at 50 000 K and 1000 more steps of cooling the system slowly to 0 K (the time step being 0.015 ps and the temperature step being 250 K). A second slow-cool annealing was then carried out in Cartesian space with the system temperature decreased from 2000 to 0 K in 3000 steps (the time step being 0.005 ps and the temperature step being 25 K). Finally, a 3000-step Powell minimization was performed to obtain the last conformation. This conformation was checked for violations of geometric and experimental restraints and atom overlapping. If there were no severe restraint violation and/or atom overlapping, it was accepted by the program as possible solution. Whether this conformation was accepted, it would be used as the starting conformation for the next cycle of simulation. The initial velocities were randomly set according to the Maxwell distribution at the starting temperature; therefore, the sampling would not be trapped in a local minimum. The simulation was repeated until enough conformations had been accepted. During one particular cycle, the weighting factor for the van der Waals energy was increased from 0.1 to 4.0, which also facilitated in transferring the system to different conformations at the beginning of the simulation.

Although this procedure is not an iterative one itself, we repeated it for several trials. There were some NOE peaks that could not be assigned unambiguously at the beginning of our calculation due to chemical shift overlapping. Some of them were imposed as summation-averaged distance restraints (*31*), while the others were not used until they could be assigned with the help of intermediate structures.

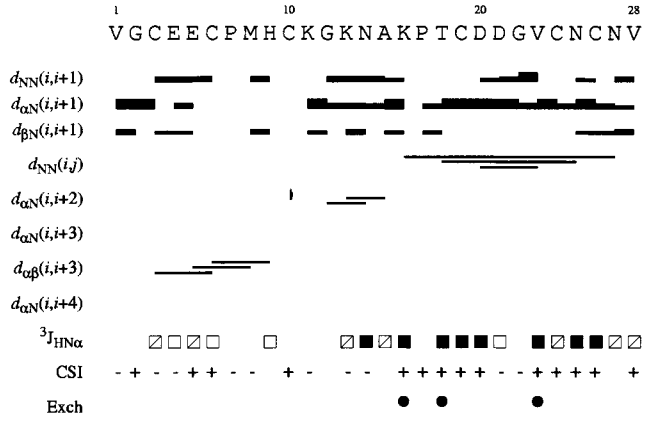

FIGURE 2: Sequence of BmP02 and NMR data used for secondary structure identification. The data are derived from NOESY and DQF-COSY spectra recorded at pH 4.0 and 300 K. The H−D exchange experiments were performed at 283 K. $^3J_{HN\alpha} \leq 6.5$ Hz (□); 6.5 Hz $\leq {}^3J_{HN\alpha} \leq 8$ Hz (▨), and $^3J_{HN\alpha} > 8$ Hz (■). CSI (*36*): (+) positive index, indicating chemical shifts larger than the corresponding random-coil values; (−) negative values.

RESULTS AND DISCUSSION

Sequential Assignment. Spin systems were identified on the basis of both the TOCSY and DQF-COSY spectra. Some ambiguities due to overlapping signals were solved by the comparative use of spectra recorded at two temperatures, 300 and 310 K. The unique Ala15 and Thr18 were identified according to the patterns of their cross-peaks on TOCSY and DQF-COSY, while His9 was identified using intraresidual NOE cross-peaks between its two Hβ and the Hδ_2 protons on the imidazole ring. Starting from Ala15, we linked it up to Lys16 and down to Lys11; starting from Thr18, we linked it with Cys19. One of the two spin systems corresponding to Pro had weak cross-peaks with both Lys16 and Thr18. The peaks were then assigned to HN−H$\delta_{i,i+1}$ and Hβ−HN$_{i,i+1}$ correlation peaks, and that spin system was assigned as Pro17 while the other as Pro7. Besides Gly12 that had been assigned, there were two other glycine residues (Gly2 and Gly22). From one of them, it was easy to establish the sequential linkage from Asp20 to Val28, based on Hα−HN$_{i,i+1}$ connectivities and confirmed by HN−HN$_{i,i+1}$ or Hβ−HN$_{i,i+1}$ connectivities. Another glycine was connected with Val1, which lacked the HN signal, and Cys3, which was linked further to Glu4 and Glu5. The HN signal from Cys6, Met8, and Cys10 could not be found unambiguously on the spectra at 300 K. After checking the spectra at 310 K, we identified Cys6, which had HN−HN$_{i,i+1}$ connectivity with Glu5 and HN−H$\delta_{i,i+1}$ connectivity with Pro7, and Met8, which had HN−HN$_{i,i+1}$ and Hβ−HN$_{i,i+1}$ connectivities to His9. We could not find any unambiguous cross-peak between Cys10 and His9/Lys11, but there was a remaining unassigned AMX spin system, whose HN overlapped with both His9 and Lys11; it was then assigned as Cys10. On the NOESY spectra recorded at 310 K, the two HNs from Cys19 and Asp20 were distinguished, and the strong NOE peak between 19Hα and 20HN could be observed unambiguously. Finally, a nearly complete assignment of all the protons was obtained (Figure 2 and Table S1 and Figure S1 in the Supporting Information).

Coupling Constants. Nineteen $^3J_{HN\alpha}$ values were obtained, as listed in Table S1. Thirteen of them were converted into ϕ angle constraints, the others being in the range between 6.5 and 8.0 Hz. Among the nine residues for which we failed to obtain coupling constants, there were three glycines, two prolines, the first valine, and residues 8, 10, and 11 for which no suitable peaks with enough signal to noise could be used.

Secondary Structures. Analysis of the sequential and medium-range NOE intensities together with the chemical shifts and coupling constant values helped us to depict the secondary structure of BmP02 (Figure 2). Two stretches of strong sequential Hα−HN NOEs indicated two extended regions running from residues 17 to 21 and 23 to 26. HN−HN connectivities were identified between residues 20 and 23, 18 and 25, and 16 and 27, with decreasing intensities. Thus, we suggested that an antiparallel β-sheet centered at residues 21 and 22 runs from residues 17 to 26. This was confirmed by the chemical shift index and the relatively large coupling constants for the residues located in the two strands.

Most other short chain scorpion toxins, like P01 and P05, have a α-helix in the N-terminus. But we could not find the characteristic Hα−HN$_{i,i+3}$ and Hα−HN$_{i,i+4}$ connectivities in BmP02, although we did observe a stretch of strong HN−HN$_{i,i+1}$ NOEs in this region. The chemical shift index also failed to predict this helix since there were no continuous −1 indexes for four residues.

Hydrogen Bonds. The rates of exchange of amide protons with solvents were measured. Amide protons present after 7 h of exchange were considered slowly exchanging amide protons, which may be engaged in hydrogen bonds. In our experiments, only the HN of residues 23, 16, and 18 gave rise to cross-peaks on the NOESY spectrum after 7 h of exchange. Some preliminary calculations confirmed the existence of the β-sheet and indicated that 23HN and 18HN formed hydrogen bonds with CO of residues 20 and 25, respectively. Thus, we included these two hydrogen bonds in structure calculations at an early stage. During the calculation, we found that 20HN also formed hydrogen bonds, which was suggested consistently by all the intermediate structures. The amide proton of Asp20 still gave rise to cross-peaks after 1 h of exchange, so we added this hydrogen bond, too. The hydrogen receptor for the HN of Lys16 was identified as one of the two terminal CO groups of residue 28 until the next-to-last run, when most of the ambiguous NOEs had been included as restraints.

Stereospecific Assignment. Stereospecific assignments for β-methylene protons were made for four residues of the 14 nondegenerate proton pairs (residues 16, 20, 21, and 26; see Table S1) according to intraresidue and sequential NOEs and $^3J_{\alpha\beta}$ coupling constants, carried out in the HABAS (*32*) routine in DYANA (*33*). The two Hα protons of Gly22 and the β-protons of Glu5 were also included stereospecifically during the calculation, according to the consistent differences in their NOEs with other protons and the corresponding distances calculated from intermediate conformations. For those remaining prochiral pairs of protons and other ambiguous NOEs, their r^{-6} summation-averaged distances were constrained during the simulation, with the upper limit converted from the sum of the two NOE intensities.

Structure Calculations. The final set of constraints contained 92 intraresidue, 68 sequential, 14 medium-range, and 20 long-range distance constraints (Figure 4), together with 13 angle constraints and seven distance constraints derived from four hydrogen bonds and three disulfide bonds. From

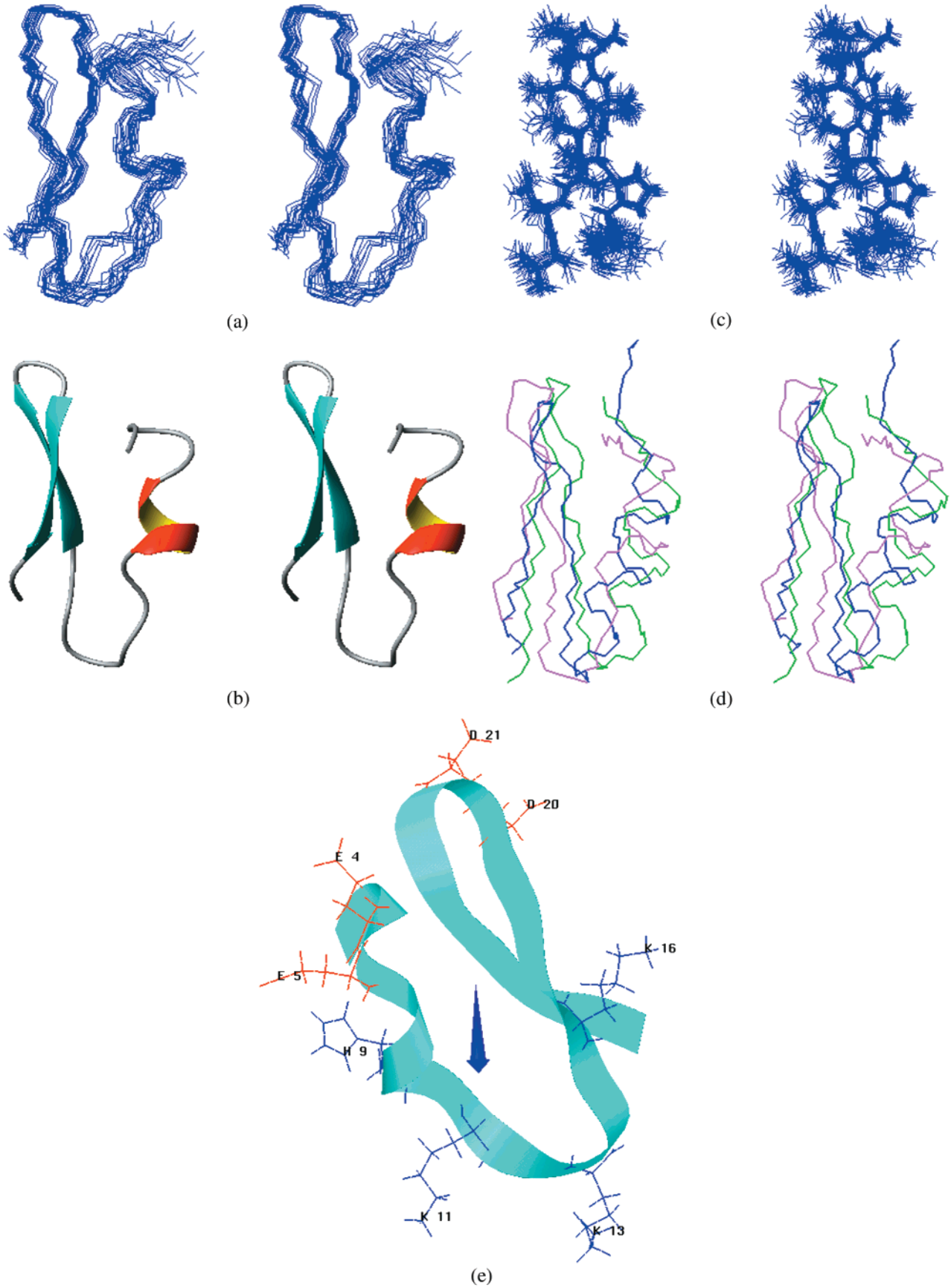

FIGURE 3: Stereoview of (a) the backbone superimposition of the 25 models for BmP02, (b) the ribbon representation of the minimized average structure of BmP02, (c) the superimposition of the best defined fragment (residues 15−28) in BmP02, where both the backbone and side chains are shown, and (d) the backbone superposition of BmP02 (in red) with P01 (in green) and P05 (in blue) (the structures of P01 and P05 were derived from PDB files 1pnh and 1scy, respectively). (e) Representation of the dipole moment of BmP02. Only the backbones are represented (cyan ribbons) with the side chains of charged residues in red (acidic) or blue (basic). The arrow indicates the orientation of the dipole moment. Panels a−d were produced with MOLMOL (*42*), while panel e was produced with GRASP (*43*).

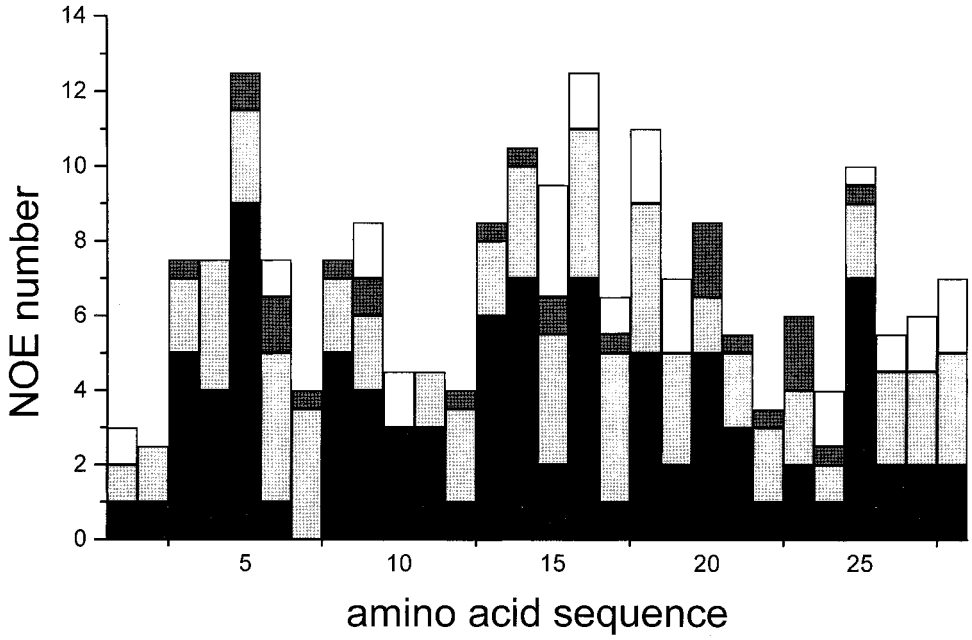

FIGURE 4: Plot of the number of NOE constraints per residue used in the calculation of the BmP02 structure vs the sequence of BmP02. Filled, shadowed, hatched, and open bars represent intraresidual, sequential, medium-range, and long-range NOEs, respectively.

Table 1: Structural Statistics for the 25 Conformers Used To Represent the Solution Structure of BmP02 before and after the 100 Steps of Powell Minimization with Full van der Waals Energy

	A[a]	B[a]
energy (kcal/mol)		
total	-52.4 ± 8.9	-71.7 ± 7.4
bonds	2.3 ± 0.4	4.1 ± 0.5
angles	16.1 ± 1.3	21.1 ± 1.9
improper	0.6 ± 0.2	1.3 ± 0.3
van der Waals	-21.3 ± 6.1	-49.9 ± 4.9
electrostatic	-62.8 ± 5.1	-64.3 ± 4.7
NOE	12.6 ± 1.8	16.1 ± 2.1
Cdih	$(6.8 \pm 3.9) \times 10^{-3}$	$7.4 \times 10^{-4} \pm 2.4 \times 10^{-3}$
residual NOE distance constraint violations (Å)		
no. >0.1 Å	5.6/194	7.5/194
rmsd	0.029	0.033
maximum	0.27	0.30

[a] The structures were obtained initially using simulated annealing followed by 3000 steps of Powell minimization with pure-repel van der Waals energy (A). One hundred more steps of Powell minimization using the full van der Waals led to few changes in the conformations and a much lower van der Waals energy (B).

the 50 accepted conformations, the 24 structures with minimal NOE violations and the lowest total energy were selected. These 24 conformations, together with their minimized average conformation, formed our solution for the structure of BmP02. All these 25 conformations are in good agreement with the experimental data, with no distance violations larger than 0.3 Å and no angle violations of more than 5°. Only four of these conformations had one distance violation larger than 0.20 Å. The covalent geometry was respected as indicated by the low-energy values of the bond lengths and valence angles. The negative van der Waals energy indicates the absence of nonbonded contacts. The van der Waals energy could be lowered dramatically after 100 steps of Powell minimization considering the complete van der Waals energy and electrostatic energy, while other energies were increased slightly. After this minimization, the conformation changed slightly, with a typical rmsd for all the heavy atoms of 0.09 Å (Table 1). A Ramachandran plot was produced by PROCHECK-NMR (*41*), which showed that 65.1% of the residues are in the most favored regions and 29.1 and 5.7% in additional and generously allowed regions, respectively (Figure S3a).

Table 2: Root-Mean-Square Deviations of the Structure Assembly of BmP02

pairwise rmsds for residue 1−28 (Å)	
backbone	1.25 ± 0.29 (0.55−1.95)
heavy atoms	1.94 ± 0.31 (1.07−2.62)
rmsds from the mean structure (backbone/heavy atoms) (Å)	
residues 1−28	0.87/1.66
residues 2−28	0.79/1.60
residues 2−9 and 14−28	0.63/1.25
residues 14−28	0.33/1.01
residues 2−9	0.39/1.21

Table 2 lists the position rmsds for backbone and all heavy atoms among the 25 structures. As can be seen from Table 2, the rmsd for the whole molecule is relatively large (0.87 Å for backbone atoms), and the value drops significantly (to 0.63 Å) when residues 1 and 10−13 were excluded from the calculation.

Structure Description. Figure 3b shows the ribbon representation for the minimized average structure of BmP02. Like other short chain scorpion toxins, BmP02 possesses an α-helix (residues 6−9) connected to an antiparallel β-sheet (residues 17−26) by two disulfide bridges.

The β-hairpin was well-defined, as evidenced from the low rmsd for this region (Table 2), the superimposition of the region shown in Figure 3c, and the ∼1 angular order parameters (*34*) (Figure S2 in the Supporting Information). The sheet was right-hand-twisted. The turn, as analyzed by the criteria described by Wilmot et al. (*35*), is close to a type I′ β-turn. The presence of a proline at position 17 might prevent the sheet from extending further, and the amide of Lys16 formed a hydrogen bond with the carboxyl of Val28.

The α-helix, which was seen until the last stage, is not so well defined, as evidenced by the low angular order parameters (Figure S2). It is short (only one turn), is distorted in the two ends, and may be not very rigid. The hydrogen bonds stabilizing it may break during conformation fluctuations. This might result in the HN signal vanishing before it can be detected in the H/D exchange experiments. The HN signals from residues 6, 8, and 10 were significantly weaker in 300 K spectra than in 310 K spectra, which could be attributed to the chemical exchanges of these residues among different local conformations (especially, between H-bond forming and breaking). Residues 3−5 also adopted a helix-like conformation, although even more distorted.

Both the N-terminal and C-terminal parts did not run far away from the major part of BmP02. As mentioned above, the C-terminal valine formed a hydrogen bond with the amide of Lys16 through one of its carboxyl oxygens. The N-terminal Val folded back toward the second β-strand and the helix, and the side chain methyls reached out to the aromatic ring of His9.

Comparison with P01 and P05. As can be seen from the backbone superposition of BmP02 with P01 and P05 (Figure 3d), BmP02 adopted a conformation different from P05 and P01 in the N-terminal part. Its helix was much shorter, while the following loop was longer and more poorly defined. In fact, the whole α/β structure in BmP02 was nearly destroyed. Unlike P01 and P05, in which the helices run nearly parallel to the β-sheet (with a cross angle of ∼10°), BmP02 has a helix running from one side of the β-sheet to another side (the cross angle being ∼50°).

The proline at position 17 of BmP02 is unusual. Most scorpion toxins contain a glycine at this site, such as charybdotoxin and leiurotoxin I. It was suggested that the glycine should be conserved in a α/β motif due to steric hindrance between the helix and the sheet (*11*). Later studies found that the replacement of this Gly with an Ala did not disturb the global fold significantly, as in noxiustoxin, margatoxin, maurotoxin, and P01. It appeared that the methyl side chain of the alanine could be accommodated when the helix was bent slightly (*38*).

We suppose that the α-helix shifts toward the second β-strand to avoid overlapping with the bulky side chain of Pro17. This shift was accomplished mainly by a rotation of ∼40° with Cys6 unmoved. The rotation led the end of the α-helix away from the beginning of the first β-strand. Therefore, residues 11−13 might fail to extend as a helix due to covalent restriction. In the case of residues 3−5, they were bent a little so that they would not go too far from the β-sheet to form the disulfide between Cys3 and Cys19. Because the size of interaction surface between the α-helix and the β-sheet was dramatically reduced by this rotation, it was not surprising to observe the relative position between them fluctuating moderately (for evidence, see the rmsds in Table 2 and Figure 3a). This also hinted that the three disulfides were not enough for a stable α/β fold; other interactions, including hydrophobic interactions, were also important.

The amide exchange rate looks quite fast compared with the usual rates observed for related molecules (*15*, *16*). It is an indication of the structure instability of BmP02, including the β-sheet. Due to lack of intense hydrophobic interactions with other parts, the β-sheet might be subject to conformation fluctuations accompanied by hydrogen bond breaking, although at a much slower rate than other parts in BmP02.

Conformational Heterogeneity. The calculated conformer ensemble of BmP02 indicated that the region of residues 10−14 was weakly defined, as can be seen from the backbone superimposition in Figure 3a. The residues of this region exhibited the largest rmsd (Figure S3b). This could partly be attributed to the failure to distinguish the overlapped HN chemical shifts of His9, Cys10, and Lys11. Since no NOE cross-peaks between His9 and Cys10 or between Cys10 and Lys11 could be used in the structure calculation, φ of His9, ϕ and φ of Cys10, and ϕ of Lys11 were not effectively constrained. However, evidence that indicating conformational heterogeneity of this region also exists. We observed the NOE cross-peaks from both Hα protons of Gly12 to HN of Gly12 and Lys13, and NOEs between amide protons of Gly12 and Lys13. All five of these peaks were strong or moderately strong. They could not be satisfied in one single conformer. The resonance of amides from Lys13 and Asn14 seemed to consist of more than one frequency, which should not be attributed to scalar coupling since these frequencies had different contributions in different peaks. Inspection of the α-proton chemical shifts of BmP02 showed a continuous fragment from residue 9 to residue 15 where the chemical shift deviation from random coil values was small (less than 0.10 ppm for residues 10, 11, 13, and 15 and less than 0.15 ppm for three more). This is consistent with the relatively low backbone angular order parameters for this region (Figure S2), and suggests that fluctuations among different conformations of this loop must occur so that averaged chemical shifts were observed (*39*).

Structure−Function Relation. It was proposed that the way such scorpion toxins approach their target potassium channel be determined by the whole charge repartition on the toxin (*38*, *40*). Figure 3e shows the dipole orientation for BmP02. It clearly demonstrates that side chains of K11 and K13 are most probably involved in the electrostatic interactions with ion channels. The side chain of K16 points to another direction and may not interact with the target ion channel. This explains the fact that BmP03, another toxin from *B. martensi* Karsch that is different from BmP02 by only one residue replacement (K16N), has a very similar affinity for the same target (*21*). The relatively weak toxicity of BmP02 must be associated with the instability of the binding region centered at K11 and K13. In another respect, this region could adopt different conformations to interact with different targets.

In conclusion, we demonstrated how a single residue has distorted the whole α/β fold of a scorpion toxin. The results must be instructive for engineering the scorpion toxin scaffolds into functional miniproteins.

ACKNOWLEDGMENT

We thank Dr. P. Güntert and Prof. K. Wüthrich for providing the programs PROSA and DYANA. We thank Dr. C. Bartels and K. Wüthrich for providing XEASY. We thank Dr. R. Koradi and K. Wüthrich for providing MOLMOL. We thank Dr. A. T. Brünger for providing the program CNS.

SUPPORTING INFORMATION AVAILABLE

Table S1 with chemical shifts of BmP02 protons, Figure S1 showing sequential connectivity in the Hα−HN and HN−HN regions, Figure S2 showing the α-proton chemical shifts versus backbone angular order parameters, and Figure S3 showing Procheck analysis results of the calculated structure of BmP02. This material is available free of charge via the Internet at http://pubs.acs.org.

REFERENCES

1. Rochat, H., Bernard, P., and Couraud, F. (1979) *Adv. Cytopharmacol. 3*, 325−334.
2. Caterall, W. A. (1980) *Annu. Rev. Pharmacol. Toxicol. 20*, 15−43.
3. Martin-Eauclaire, M. F., and Couraud, F. (1995) in *Handbook of Neurotoxicology* (Chang, L. W., and Dyer, R. S., Eds.) pp 683−716, Dekker, New York.
4. Gimenez, G., Navia, M. A., Reuben, J. P., Katz, G. M., Kaczorowshi, G. J., and Garcia, M. L. (1988) *Proc. Natl. Acad. Sci. U.S.A. 85*, 3329−3333.
5. Crest, M., Jacquet, G., Gola, M., Zerrouk, H., Benslimane, A., Rochat, H., Mansuelle, P., and Martin-Eauclaire, M. F. (1992) *J. Biol. Chem. 267*, 1640−1647.
6. Possani, L. D., Martin, B. M., and Svendsen, I. (1982) *Carlsberg Res. Commun. 47*, 285−289.
7. Galvez, A., Gimenez, G., Reuben, J. P., Ray-Contanain, L., Feigenbaum, P., Kaczorowski, G. J., and Garcia, M. L. (1990) *J. Biol. Chem. 265*, 11083−11090.
8. Auguste, P., Hugues, M., Gravé, B., Gesquière, J.-C., Maes, P., Tartar, A., Romey, G., Schweitz, H., and Lazdunski, M. (1990) *J. Biol. Chem. 265*, 4753−4759.
9. Zerrouk, H., Mansuelle, P., Benslimane, A., Rochat, H., and Martin-Eauclaire, M. F. (1993) *FEBS Lett. 320*, 189−192.
10. Zerrouk, H., Laraba-Djebari, F., Fremont, V., Meki, A., Darbon, H., Mansuelle, P., Oughideni, R., Van Rietschoten, J., Rochat, H., and Martin-Eauclaire, M. F. (1996) *Int. J. Pept. Protein Res. 48*, 514−521.
11. Bontems, F., Roumestand, C., Boyot, P., Gilquin, B., Doljansky, Y., Ménez, A., and Toma, F. (1991) *Eur. J. Biochem. 196*, 19−28.
12. Fernández, I., Romi, R., Szendeffy, S., Martin-Eauclaire, M. F., Rochat, H., Van Rietschoten, J., Pons, M., and Giralt, E. (1994) *Biochemistry 33*, 14256−14263.
13. Dauplais, M., Gilquin, B., Possani, L. D., Gurrola-Briones, G., Roumestand, C., and Menez, A. (1995) *Biochemistry 34*, 16563−16573.
14. Martins, J. C., Van De Ven, F. J. M., and Borremans, F. A. M. (1995) *J. Mol. Biol. 253*, 590−603.
15. Meunier, S., Bernassau, J.-M., Sabatier, J.-M., Martin-Eauclaire, M. F., Van Rietschoten, J., Cambillau, C., and Darbon, H. (1993) *Biochemistry 32*, 11969−11976.
16. Blanc, E., Fremont, V., Sizun, P., Meunier, S., Van Rietschoten, J., Thevand, A., Bernassau, J.-M., and Darbon, H. (1996) *Proteins 24*, 359−369.
17. Vita, C., Drakopoulou, E., Vizzavona, J., Rochette, S., Martin, L., Menez, A., Roumestand, C., Yang, Y. S., Ylisastigui, L., Benjouad, A., and Gluckman, J. C. (1999) *Proc. Natl. Acad. Sci. U.S.A. 96*, 13091−13096.
18. Vita, C., Roumestand, C., Toma, F., and Menez, A. (1995) *Proc. Natl. Acad. Sci. U.S.A. 92*, 6404−6408.
19. Vita, C., Vizzavona, J., Drakopoulou, E., Zinn-Justin, S., Gilquin, B., and Menez, A. (1998) *Biopolymers 47*, 93−100.
20. Romi-Lebrun, R., Martin-Eauclaire, M. F., Escoubas, P., Wu, F. Q., Lebrun, B., Hisada, M., and Nakajima, T. (1997) *Eur. J. Biochem. 245*, 457−464.
21. Tong, Q. C., Zhang, Y., Li, D., Zhou, Z. N., and Ji, Y. H. (2000) *Regul. Pept. 90* (1−3), 85−92.
22. Sabatier, J.-M., Zerrouk, H., Darbon, H., Mabrouk, K., Benslimane, A., Rochat, H., Martin-Eauclaire, M.-F., and Van Rietschoten, J. (1993) *Biochemistry 32*, 2763−2770.
23. Marion, D., Ikuto, M., Tschudin, P., and Bax, A. (1989) *J. Magn. Reson. 85*, 393−399.
24. Macura, S., Huang, Y., Suter, D., and Ernst, R. R. (1981) *J. Magn. Reson. 43*, 259−281.
25. Piotto, M., Saudek, V., and Sklenar, V. (1992) *J. Biomol. NMR 2*, 661−665.
26. Güntert, P., Dötsch, V., Wider, G., and Wüthrich, K. (1992) *J. Biomol. NMR 2*, 619−629.
27. Wüthrich, K. (1986) in *NMR of proteins and nucleic acids*, John Wiley & Sons, New York.
28. Bartels, C., Xia, T.-H., Billeter, M., Güntert, P., and Wüthrich, K. (1995) *J. Biomol. NMR 5*, 1−10.
29. Szyperski, T., Güntert, P., Otting, G., and Wüthrich, K. (1992) *J. Magn. Reson. 99*, 552−560.
30. Brünger, A. T., Adams, P. D., Clore, G. M., Delano, W. L., Gros, P., Grosse-Kunstleve, R. W., Jiang, J.-S., Kuszewski, J., Nilges, M., Pannu, N. S., Read, R. J., Rice, L. M., Simonson, T., and Warren, G. L. (1998) *Acta Crystallogr. D54*, 905−921.
31. Nilges, M. (1993) *Proteins 17*, 297−309.
32. Güntert, P., Braun, W., and Wüthrich, K. (1991) *J. Mol. Biol. 217*, 517−530.
33. Güntert, P., Mumenthaler, C., and Wüthrich, K. (1997) *J. Mol. Biol. 273*, 283−298.
34. Hyberts, S. G., Goldberg, M. S., Havel, T. F., and Wagner, G. (1992) *Protein Sci. 1*, 736−751.
35. Wilmot, C. M., and Thornton, J. M. (1988) *J. Mol. Biol. 203*, 221−232.
36. Wishart, D. S., Sykes, B. D., and Richards, F. M. (1992) *Biochemistry 31*, 1647−1651.
37. Wishart, D. S., Bigam, C. G., Holm, A., Hodges, R. S., and Sykes, B. D. (1995) *J. Biomol. NMR 5*, 67−81.
38. Blanc, E., Sabatier, J. M., Kharrat, R., Meunier, S., ElAyeb, M., Van Rietschoten, J., and Darbon, H. (1997) *Proteins 29*, 321−333.
39. Wishart, D. S., and Sykes, B. D. (1994) *Methods Enzymol. 239*, 363−392.
40. Blanc, E., Lecomte, C., Van Rietschoten, J., Sabatier, J. M., and Darbon, H. (1997) *Proteins 29*, 359−369.
41. Laskowski, R. A., Rullmann, J. A. C., MacArthur, M. W., Kaptein, R., and Thornton, J. M. (1996) *J. Biomol. NMR 8*, 477−486.
42. Koradi, R., Billeter, M., and Wüthrich, K. (1996) *J. Mol. Graphics 14*, 51−55.
43. Nicholls, A., Sharp, K. A., and Honig, B. (1991) *Proteins 11*, 281−296.

BI000860S